+ MODEL
ARTICLE IN PRESS
+ MODEL
Available online at www.sciencedirect.com
ScienceDirect
Publishing Services by Elsevier
International Journal of Naval Architecture and Ocean Engineering xx (2016) 1—14
http://www.journals.elsevier.com/international-journal-of-naval-architecture-and-ocean-engineering/

Numerical optimization of Wells turbine for wave energy extraction

Paresh Halder [a], Shin Hyung Rhee [b], Abdus Samad [a,b,*]

[a] *Wave Energy and Fluid Engineering Laboratory, Department of Ocean Engineering, Indian Institute of Technology Madras, Chennai 600036, India*
[b] *Research Institute of Marine Systems Engineering, Department of Naval Architecture and Ocean Engineering, Seoul National University, Seoul, South Korea*

Received 5 May 2016; revised 20 June 2016; accepted 27 June 2016
Available online ■ ■ ■

Abstract

The present work focuses multi-objective optimization of blade sweep for a Wells turbine. The blade-sweep parameters at the mid and the tip sections are selected as design variables. The peak-torque coefficient and the corresponding efficiency are the objective functions, which are maximized. The numerical analysis has been carried out by solving 3D RANS equations based on *k-w* SST turbulence model. Nine design points are selected within a design space and the simulations are run. Based on the computational results, surrogate-based weighted average models are constructed and the population based multi-objective evolutionary algorithm gave Pareto optimal solutions. The peak-torque coefficient and the corresponding efficiency are enhanced, and the results are analysed using CFD simulations. Two extreme designs in the Pareto solutions show that the peak-torque-coefficient is increased by 28.28% and the corresponding efficiency is decreased by 13.5%. A detailed flow analysis shows the separation phenomena change the turbine performance.

Keywords: Blade sweep; Wells turbine; Optimization; Wave energy; CFD

1. Introduction

In the recent years, various renewable energy sources have been explored, and devices to harness such energy are developed. One such device is an Oscillating Water Column (OWC) to harvest ocean wave energy. The device uses a Wells turbine for its power-take off. The turbine is an axial-flow self-rectifying low-pressure turbine and rotates continuously in a unique direction by the bidirectional action of air or working fluid. The turbine blades have a stagger angle of 90° and are constructed using symmetric aerofoils.

In the OWC, a reciprocating airflow is created by the action of ocean waves and the air transfers energy to the turbine blades. The air, which is the working fluid, reverses its direction with wave but the turbine rotation direction does not change. The effect of turbine design parameters have been investigated based on the experimental and numerical analysis by several researchers (Brito-Melo et al., 2002; Raghunathan, 1995; Taha et al., 2010; Torresi et al., 2004; Halder et al., 2015). However, there exists a limited number of systematic optimization works to improve its design and performance. One of such design parameters is the aerofoil shape of the turbine blade, which is optimized to increase the power output and efficiency (Mohamed et al., 2011).

The power output and the efficiency of the turbine depend on the design parameters and nature of flow over the blade Suction Surface (SS). The power transferred to the blade is higher for the flow attached to SS. A backward swept blade has a higher efficiency and torque over a wider operating range (Webster and Gato, 2001, 1999a). The blade efficiency or performance can be altered by modifying its shape (Kim et al., 2002; Mohamed and Shaaban, 2013, 2014).

Modifications of blade shape have been reported for gas turbine, steam turbine and hydro turbine, where the researchers achieve the asymptotic enhancement of turbine

* Corresponding author. Department of Ocean Engineering, Indian Institute of Technology Madras, Chennai 600036, India.
E-mail address: samad@iitm.ac.in (A. Samad).
Peer review under responsibility of Society of Naval Architects of Korea.

http://dx.doi.org/10.1016/j.ijnaoe.2016.06.008

Nomenclature

Abbreviations

CFD	computational fluid dynamics
CV	cross validation
FC	flow coefficient
KRG	Kriging method
LE	leading edge
MOO	multi-objective optimization
NSGA	non-dominated sorting of genetic algorithm
OWC	oscillating water column
PBA	PRESS-based average
PoF	Pareto optimal front
PS	pressure surface
RANS	Reynolds-averaged Navier–Stokes
RB	rotor blade
RBF	radial basis function
Ref	reference
RSA	response surface analysis
SS	suction surface
SST	shear stress transport
TC	tip clearance
TE	trailing edge
TKE	turbulent kinetic energy
WAS	weighted average surrogate

Symbols

B	rotor axial length
C	rotor blade chord length
d_1	constant of equation (2)
d_2	constant of equation (2)
E	error
F	objective function
$h = \frac{R_{hub}}{R_{tip}}$	hub-to-tip ratio
N	speed of rotor, rpm
N_{sm}	the number of basic surrogate model
$T^* = \frac{T}{\rho\omega^3 R_{tip}^5}$	torque coefficient
$\Delta P^* = \frac{\Delta P^o}{\rho\omega^2 R_{tip}^2}$	pressure drop coefficient
ΔP^o	static pressure drop
Q	volume flow rate
$r^* = \frac{R}{R_{tip}}$	non-dimensional radius
R	radius
$R_{mid} = \frac{(1+h)}{2} R_{tip}$	mid-span radius
$s = \frac{ZC}{2\pi R_{mid}}$	turbine solidity
T	blade thickness
T	shaft torque
U_{tip}	rotor velocity
$U^* = \frac{V}{U_{tip}}$	flow coefficient
Ω	rotational speed
$U*$	flow coefficient
V	axial velocity
W	weight
z	number of rotor blades
Θ	camber angle
Λ	sweep angle
P	density
$\eta = \frac{T\omega}{Q\Delta P^o}$	efficiency
Ω	angular velocity

Subscript

1	inlet
2	outlet
A	axial
avg	average
Cv	cross validation
hub	hub
mid	mid
Sm	surrogate models
Tip	tip
was	weighted average surrogate
*	non-dimensional parameter

performance. The Wells turbine is relatively newer development and the references available on the application and performance enhancement by modifying blade shape is limited. Some key references (Table 1) show that the modifications are performed basically for blade sweep and aerofoil profile. Some researchers focused on bi-plane Wells turbine, guide vane angle, tip clearance, duct geometry modifications.

Several efficient search optimization techniques are easily available to solve the optimization problems. One such optimization technique is the surrogate based modelling, which considerably reduces the design time to optimize a system (Samad et al., 2008; Badhurshah and Samad, 2015; Goel et al., 2007; Myers and Montgomery, 1995). In the surrogate base technique, a limited number of data points are used to construct multiple surrogates to obtain the optimal design. Goel et al. (2007) developed a Weighted Average Surrogate (WAS) model to identify the regions of high uncertainty. The WAS is basically a weighted sum of basic surrogates; namely, the Response Surface Approximation (RSA) (Myers and Montgomery, 1995), the Kriging (KRG) (Jeong et al., 2005; Martin and Simpson, 2005; Sacks et al., 2012; Simpson et al., 2001; Wang et al., 2014) and the radial basis function (RBF) (Orr, 1996). Several other articles (Valipour and Montazar, 2012a, 2012b, 2012c; Valipour et al., 2013, 2012)also reports several surrogates, but those do not contain WAS model.

The real life engineering problems have multiple objectives (Deb, 2001). A Multi-Objective Optimization (MOO) consists of two or more objectives which provide better understanding about the objectives and the variables in terms of performance enhancement. This also assists the designers to determine the best design or several design alternatives. In some design problems, conflicting objectives are correlated via Pareto optimal Front (PoF) of MOO (Collette and Siarry, 2003; Marjavaara et al., 2007). Another widely used approach based on a meta-heuristic algorithm includes a non-dominated sorting of a genetic algorithm (NSGA-II). The WAS model has been implemented for NSGA-II population generation for

Please cite this article in press as: Halder, P., et al., Numerical optimization of Wells turbine for wave energy extraction, International Journal of Naval Architecture and Ocean Engineering (2016), http://dx.doi.org/10.1016/j.ijnaoe.2016.06.008

Table 1
Important modification to enhance the performance of Wells turbines.

Design modification	Advantage	Description	Profile
Sweep with and without guide vane (Brito-Melo et al., 2002)	Turbine capable of operating with good efficiency over a wide range of flow rates.	Bypass pressure-relief valve produced higher electrical energy.	NACA0015
Aerofoil shape (Mohamed et al., 2011)	Increased power output (average relative gain of +11.3%) and enhanced efficiency (1% thought the operating range)	Incident angle varied: 5 to 14°	NACA0021
Blade sweep (Webster and Gato, 1999a)	Overall efficiency improved	30° backward sweep	NACA0015
Blade sweep (Kim et al., 2002)	Improve overall performance	Blade sweep ratio: 0.25–0.75	NACA0020
Pitch angle (Mohamed and Shaaban, 2013)	Improved efficiency: 2.3% and AOP efficiency: 6.2%.	Optimum pitch angle: 0.3°	NACA0021
Pitch angle (Mohamed and Shaaban, 2013)	Average increase in efficiency: 3.4%, power: 1%.	Optimum pitch angle: 0.6°	NACA0021
End plate (Takao et al., 2007)	Improve efficiency 4%	End plate thickness: 0.5 mm and plate margin: 0–0.3 mm	NACA0020
Blade profile Thickness (Raghunathan and Tan, 1985)	The NACA0021 produced the peak efficiency. Efficiency drop: ~10% with blade roughened blade.	Thicker and modified aerofoil blades improved performance of the turbine.	NACA0024,NACA0021, NACA0015H,NACA0015, NACA0012
Blade sweep and pitch angle (Gato and Webster, 2001)	Improve turbine performance	30° backward sweep and blade pitch angle 0 to 20°	NACA0015
Blade profile (Suzuki and Arakawa, 2008)	Efficiency improved at an angle of attack <7°. Stall angle = 10° was smaller.	fan-shaped blades with different sweep angles	NACA0021, NACA0012
Blade profile (Takao et al., 2006)	Peak efficiency higher	Optimum blade profile: NACA0015	NACA0015,NACA0020CA9, HSIM 15-262133-1576
Blade geometry (Kim et al., 2001)	Stall margin is higher with higher hub to tip ratio.	Optimum blade-sweep ratio: 0.35 and solidity: ~0.67.	NACA0020
Blade profile (Thakker and Abdulhadi, 2007)	Higher power output	Preferable rotor blade profile CA9	NACA0015,NACA0020,CA9, HSIM 15-262133-1576

finite element analysis based design (Gorissen et al., 2010; Samad and Kim, 2008). In a study by Kim et al. (2002), it was concluded that a design modification of blade sweep requires a check for applicability to higher efficiency and power (Table 1).

The multi-operating point optimization is performed through the automated optimization if the computational time is low. The simulation based works impose a greater challenge to design and simulate when a complex geometry and flow are encountered. Turbomachinery flows have such complexity, and any small numerical error or irregularity in geometry or mesh can produce disastrous result. In transonic flows (Samad and Kim, 2008), the solver time steps must be changed during simulations to get a converged result. However, the Wells turbine cannot be automated with a 3D CFD code and an optimization algorithm without applying ample efforts of observing each simulation to obtain the converged solution of any individual design.

In the present work, a Wells turbine blade design-optimization via surrogate based multi-objective optimization approach coupled with 3D CFD analysis has been carried out. A dual or two-level optimization has been performed to improve the peak-torque-coefficient and the corresponding efficiency by sweeping a blade. The flow phenomenon inside the turbine passage is explained to find the reason of the enhanced performance of the turbine.

2. Numerical methodology

2.1. CFD modelling

A Wells turbine blade geometry was adopted (Torresi et al., 2008) and a CAD model was prepared for the flow/computational domain. The turbine contains eight rotor blades. A blade has a chord length of 0.125 m and NACA0015 profile. The blade has a solidity of 0.644 m, a tip radius of 0.3 m, a hub radius of 0.2 m and hub-to-tip ratio of 0.67. The tip clearance is 1% of the chord length.

The performance of the turbine (Fig. 1) was investigated by solving 3D steady, incompressible flow equations. The Reynolds-averaged Navier–Stokes (RANS) equations were discretized by the finite volume method in Ansys-CFX® v14.5 (Ansys CFX, 2010), and the *k-w* SST turbulence closure model captured the near-wall flow physics. The CFD code, which is a coupled solver, solved the fluid flow equations (for u, v, w and p) as a single system. The solution approach adopted a fully implicit discretization scheme for given time steps. The time step guided the approximate solutions and minimizes the number of iterations. To increase the accuracy in the results, high-resolution first-order advection scheme was applied to the finite-volume equations (Ansys CFX, 2010; Benini and Biollo, 2007). The maximum residual criterion was1.0E-5 for the convergence.

Please cite this article in press as: Halder, P., et al., Numerical optimization of Wells turbine for wave energy extraction, International Journal of Naval Architecture and Ocean Engineering (2016), http://dx.doi.org/10.1016/j.ijnaoe.2016.06.008

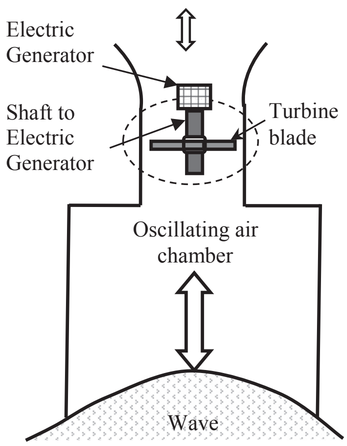

Fig. 1. Oscillating water column.

The specifications of the turbine, boundary conditions and meshing statistics are given in Tables 2 and 3. The computational domain was extended to four and six times of blade-chord lengths towards the upstream of the Leading Edge (LE) and the downstream of the Trailing Edge (TE) of the blade, respectively (Fig. 2). A single blade passage was simulated, and rotational periodic boundary conditions were applied in the circumferential direction. A rotating reference frame with a constant angular velocity was applied. The following boundary conditions were applied:

- Rotational periodicity in the circumferential direction.
- At the downstream outlet boundary (the outlet lateral-face of the computational domain): Area averaged static pressure.
- No-slip boundary conditions at blade, hub and tip.
- Uniform inlet velocity at the upstream inlet boundary.

Fig. 3 shows the mesh, which is generated in Ansys ICEM-CFD, used in the computational domain. The unstructured mesh allows the addition of blade tip clearance (TC = 1%) and was generated over the entire computational domain. The fine mesh was used in the near wall region to capture the near boundary flow physics. Ten layers of nodes were employed near the wall, so that a lower value of Y+ near the wall can be obtained. The number of grids was increased in three gradual steps from 472,823 to 815,049 nodes to check proper grid independent result and the maximum deviation of ±0.4%, ±1.55% and ±1.11% in pressure coefficient, torque coefficient and efficiency are obtained, respectively. Fig. 4 shows that the optimum number of grids is 0.6 million. The Reynolds number was approximately 5.2×10^5 at the peak efficiency point and the uncertainty of the torque coefficient was ±1.4%.

To simulate the flow, parallel processors in the Virgo super-cluster specifications of IBM System xiDataPlex dx360 M4, 2X Intel E5-2670 8C 2.6 GHz processor was used.

Table 2
Specification of the turbine model.

Parameter	Dimension
Blade profile	NACA0015
Chord length, C	0.125 m
Number of blades, z	8
Blade maximum thickness, t	15% of C
Solidity at mean radius	0.644
Casing radius	0.3 m
Hub radius	0.2 m
Mean radius	0.25 m
Tip clearance (TC)	1% of C
Turbine rotational speed	2000 rpm

Table 3
Meshing and boundary conditions.

Parameter	Description
Flow domain	Single turbine
Interface	Rotational periodic
Mesh/Nature	Unstructured
Nodes	0.6 million
Fluid nature	Air at 25 °C
Turbulence model	SST k-Ω
Inlet	Uniform inlet velocity
Outlet	Area averaged static pressure
Hub, tip and blade	No-slip
Residual convergence value	1×10^{-5}
Mass imbalance	0.001

2.2. Objective functions and design variables

In the present problem, two parameters were defined to modify the blade stacking line. These variables are the angels that modify the blade sweep at the tip section and the mid-section. The angles varied from +10° to −10° ($=\lambda_{tip}$) at the tip and from +5° to −5° ($=\lambda_{mid}$) at the mid-section (Fig. 5). The blade stacking line was defined by a third order polynomial curve to ensure a smooth change in the blade shape. The blade is swept backward if the blade tip section moves towards the TE.

The primary objective of the work was to enhance the peak-torque-coefficient and the corresponding efficiency therefore; the objective function is expressed as:

Torque coefficient:

$$T^* = \frac{T}{\rho\omega^2 R_{tip}^5} \quad (1)$$

where T is the turbine shaft torque.

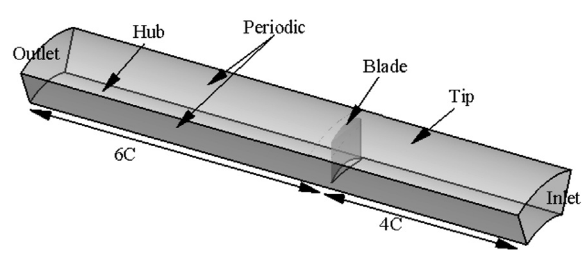

Fig. 2. Computational domain.

Efficiency:

$$\eta = \frac{T\omega}{Q\Delta P^{o}} \tag{2}$$

where Q is the volume flow rate. Where, ΔP^{o} is the static pressure drop across the turbine taking the pressure value at the inlet and the outlet of the computational domain respectively.

Both the objectives are conflicting in nature and help delay in flow separation; therefore, the blade shape optimization was used to explain the rationale behind the performance enhancement. The delayed flow separation or attached flow or the stall-delay implies that more energy is transferred to the blade. A wider operating range of a turbine is always desirable as it gives higher performance at different wave conditions. These wave conditions alter due to the change in wave height and period, which frequently occur under uneven climatic conditions for a particular sea location during the day or night.

The turbine blades faces a sinusoidal air jet as the airflow is alternating or bidirectional. Initially, the wave height increases and reaches to its crest, thereafter it changes the direction and forms a trough. As a result, the air velocity becomes zero at the crest and the trough of the wave. Fig. 6 shows the sea surface during wave-propagation, in which the air velocity is maximum at point's w2, w6 and w4. The air velocities can be zero at w1−w3, w5−w7 sections. The shaded zone near the crest and trough has less air velocity and turbine may or may not extract the appreciable amount of power from the air. The turbine-mass has its own momentum because of rotation and a fluctuation in speed can be expected due to the bidirectional airflow. At a high air-velocity zone (shaded zone), the relative tangential velocity of the blade is higher, and the turbine dissipates more energy in the air and reduces the total power output. Any effort to increase the operating zone or range would increase the total power extracting capability of the turbine during different wave heights and frequencies. Hence, the present objectives increase the operating range.

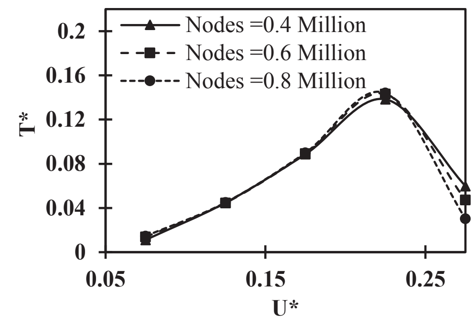

Fig. 4. Grid independency study.

To achieve a higher performance, two design variables are used to modify the blade stacking line so that the blade sections or profiles can be moved in forward or backward directions along the chord line. An angle at mid-span forms one variable (λ_{mid}) while an angle at tip forms the other variable (t_{ip}). The design parameters and the definitions of the variables are shown in Table 4 and Fig. 5b, respectively.

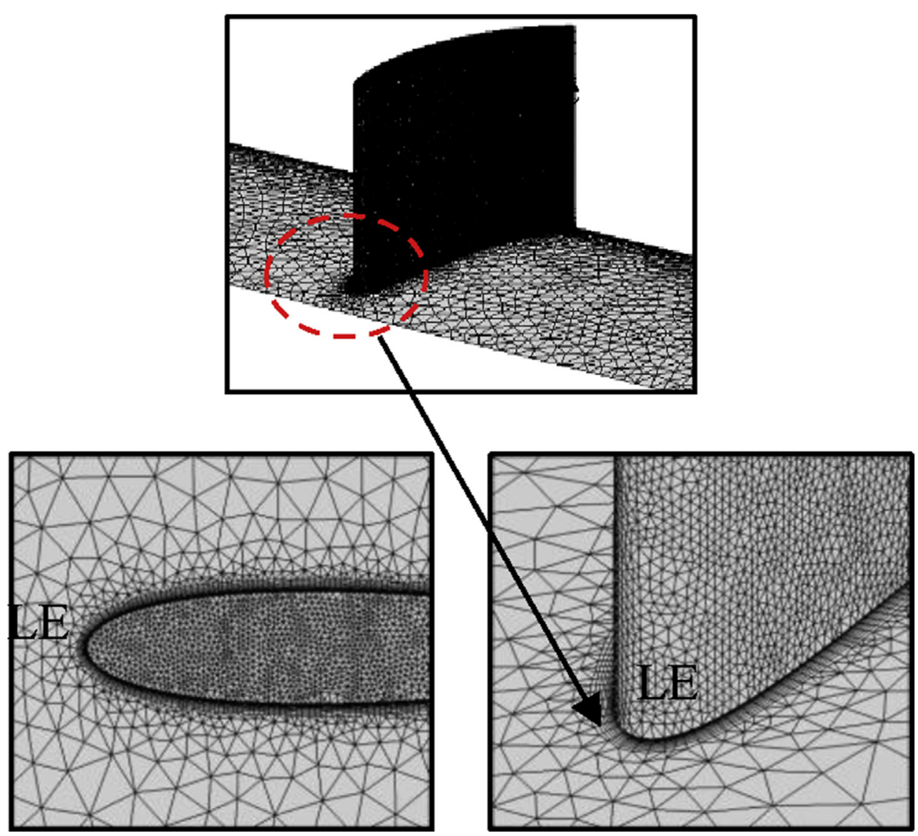

Fig. 3. Mesh on the computational domain.

+ MODEL

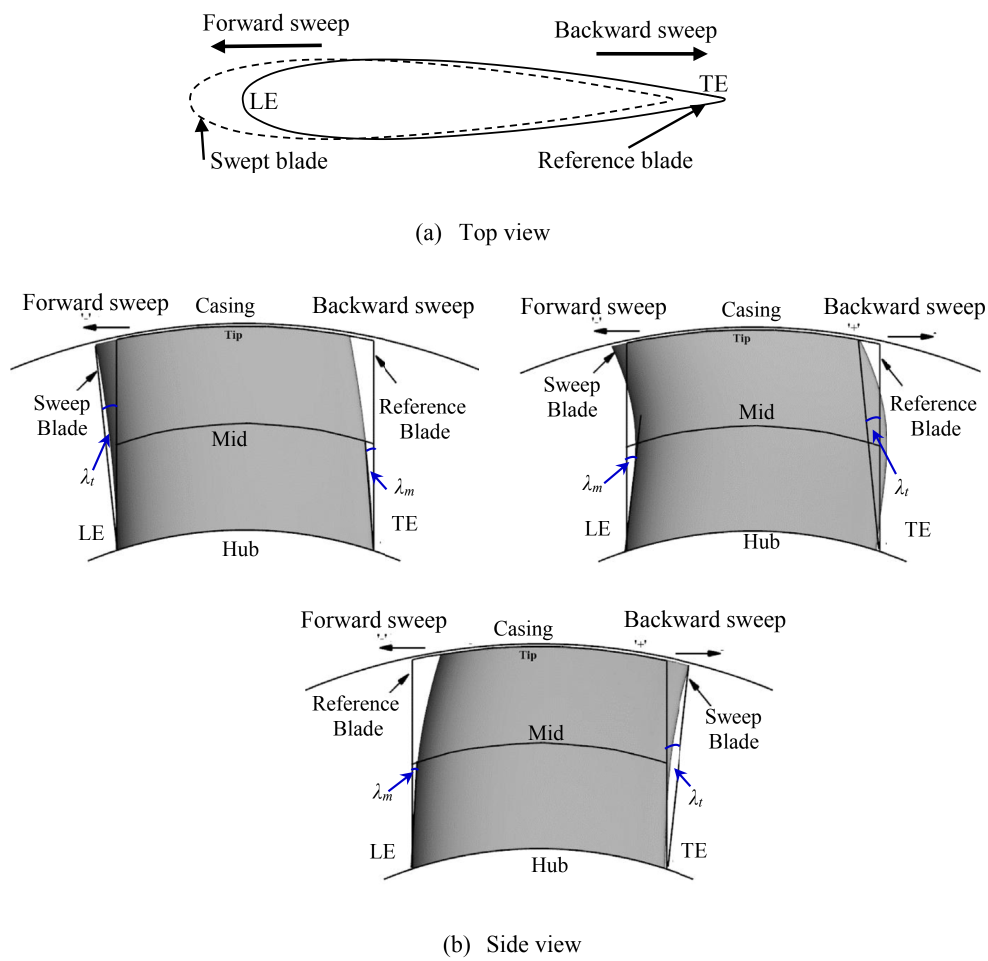

(a) Top view

(b) Side view

Fig. 5. Definition of blade sweep.

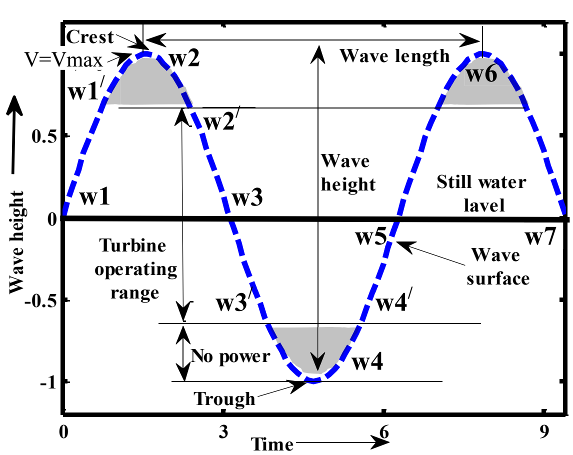

Fig. 6. Wave operating range.

Table 4
Design space of the variables.

Variable	Lower limit	Upper limit
λ_{tip}	−10	10
λ_{mid}	−5	5

The torque coefficient (T^*) and efficiency (η) were chosen as the primary objective functions. For each design, several simulations at different flow coefficients (U^*) were carried out to determine the peak-torque and the corresponding efficiency. The first step of optimization involved a single-variable, namely the flow coefficient (U^*) which was used to change the blade sweep, and the torque values were calculated. For each design, five simulations for a wider flow coefficient were carried out. Subsequently, the Bézier curves were fitted and the peak-torque and corresponding efficiency value were extracted from the curves. Each design produced a different operating range as well as the objective function values and it was noted that the peak efficiency shifted to different location of the FC axis. This implies that each design (turbine) can run at different flow velocity to give a peak-torque. Thus, a turbine that provides higher torque as well as higher efficiency is better for real life application. The turbine was operated continuously at design and off design conditions and the air velocity was varied over a wide range of operation. Hence, in the present approach, two levels of optimization are performed: a) initial level to find peak efficiency considering single objective (torque) and single parameter (U^*) and b) MOO through surrogate modelling and genetic algorithm technique. The detailed description of the complex optimization procedure or MOO is given in the following sections.

3. Optimization technique

3.1. Overview

The optimization procedure for the study is illustrated in Fig. 7. The reference geometry was created, simulated in a CFD solver and validated with existing experimental results. Then, a design space was created using the lower and the upper limits of the variables. Nine different designs or design points were selected via three-level full factorial design or design of experiments technique. These designs were simulated by the CFD solver. For each design, the solver was run for a wide range of Flow Coefficient (FC) to get the peak-torque (T^*_{max}) and the corresponding efficiency (η). The values of objective functions (T^*_{max} and η) and design variables were tabulated. During the two-level optimization procedure, the CFD simulations evaluate the initial design points for different FCs. Bézier polynomials were fitted, and values of T^*_{max} and η were obtained. For example, if we have B number of design points, we get B number of peak-torques and B number of corresponding efficiencies.

Three basic surrogates namely Response Surface Approximation (RSA), Kriging (KRG) and Radial Basis Function (RBF) were constructed and the errors related to the surrogates were evaluated via the Cross-Validation (CV) approach. The errors were used to calculate weights to construct Weighted Average Surrogate (WAS). Each objective function produced one WAS, and both the surrogates (for the both objectives) were applied as input to a controlled non-dominated sorting of genetic algorithm (NSGA-II) function. The NSGA-II produced PoF (Pareto optimal Front), which yielded several

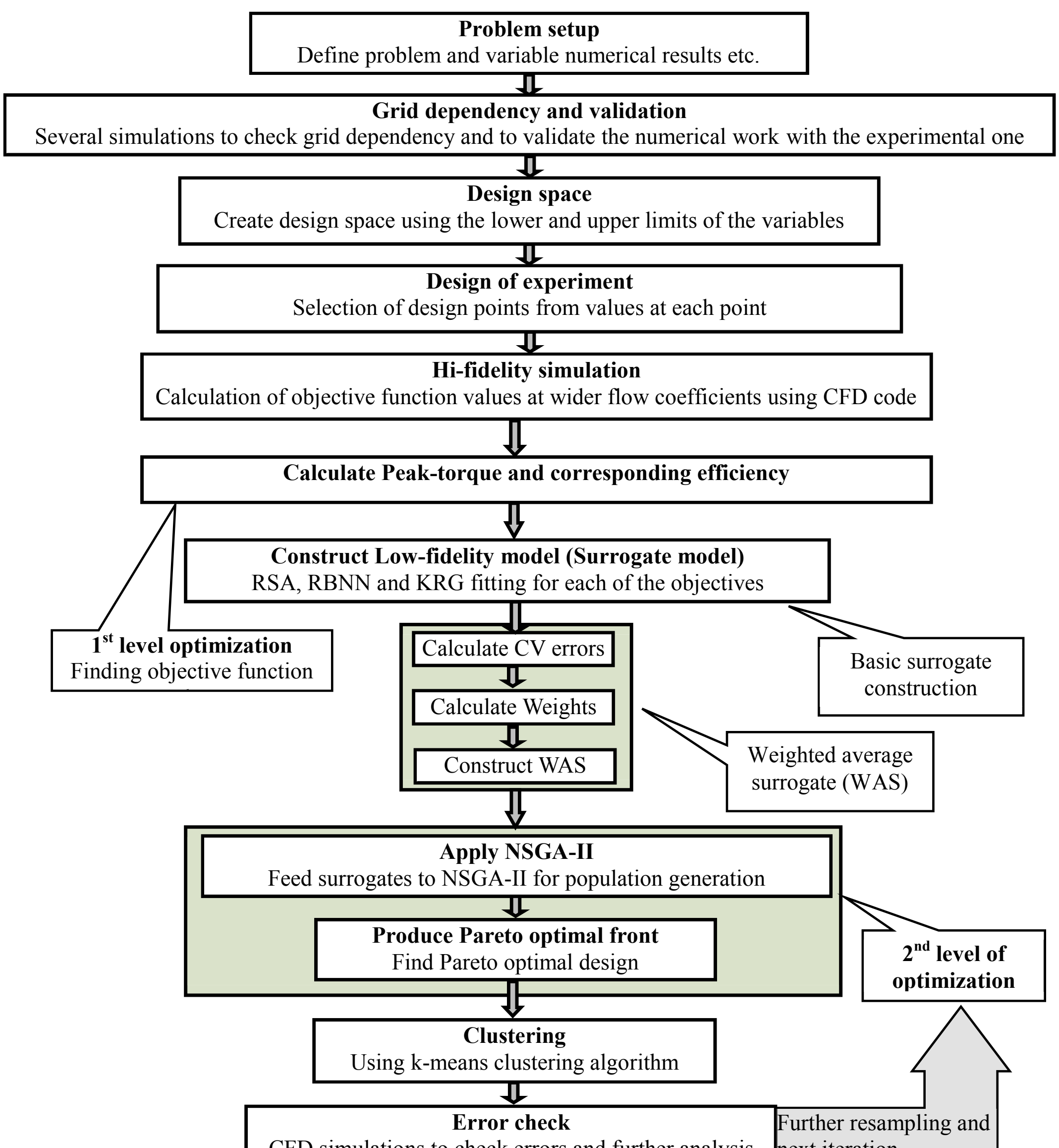

Fig. 7. Optimization procedure for the present calculations.

designs and the clustering, was obtained (Kalyanmoy Deb, 2001). Eventually, five different cluster points were selected and evaluated by CFD simulations to perform the flow analyses. This concept differs from the earlier research works (Badhurshah and Samad, 2015); which optimized the wave energy turbine system for a fixed U^*.

3.2. Surrogate models

The RSA model is an approximation technique, which uses several regression coefficients to fit a second order polynomial curve (Myers and Montgomery, 1995). In the present study, a minimum of seven data points were required to construct the RSA for two variables and six such regression coefficients were obtained. Since, KRG and RBF use less number of data points, the surrogates were constructed using nine design points only. The RBF was constructed using '*newrb*()' function of the Neural Network Toolbox of Matlab R14 (Matrices, 2012). The network has three layers: an input layer, a hidden layer and a liner output layer. These parameters define the network sensitivity or error inclusion in the output of a new dataset or design points fed into the network. Kriging method or KRG is a combination of two components: a global model and departures from the curve (Martin and Simpson, 2005). A linear regression model along with zero mean also predicts the functional behaviour of the KRG. The weighted average or WAS model (Goel et al., 2007) is a derived from the basic surrogates (RSA, KRG and RBF) and the predicted response defined by the PBA model is given below:

$$f_{was}(x) = \sum_{i}^{N_{sm}} w_i(x) f_i(x) \tag{3}$$

where N_{sm} is the number of basic surrogate models used to construct WAS. The ith surrogate at design point x produces weight $w_i(x)$, and $F_i(x)$ is the response predicted by the ith surrogate. The weighting scheme used is as follows:

$$w_i = \frac{w_i^*}{\sum_i^{N_{sm}} w_i^*}, \quad \text{where } w_i^* = \left(E_i + d_1 E_{avg}\right)^{d_2}, d_1 < 1,\ d_2 < 0, \tag{4}$$

$$E_{avg} = \sum_{i}^{N_{sm}} E_i / N_{sm},\ E_i = E_{cv,i}, \mathrm{i} = 1, 2\ 3\ \& \ldots N_{sm}$$

where E_{cv} is calculated from the leave-one-out CV error estimation (Goel et al., 2007).

3.3. Cross-validation

In CV, the data points are randomly partitioned into k equal points. A single point is retained as the validation point for testing a surrogate and the remaining k-1 points are used to construct the surrogate. The surrogate is constructed k times with each of the k designs used exactly once as the validation point. Hence, k errors were obtained and gross mean square error or CV error (E_{cv}) was calculated. A single surrogate gives exactly one E_{cv}. The E_{cv} is then used to calculate the weights of each surrogate from the Eq. (4). If k is equal to the number of data points, the CV is called leave-one-out CV.

3.4. NSGA-II and POF

A variant of NSGA-II, called controlled elitist genetic algorithm, is a Multi-Objective Optimization (MOO) algorithm (Deb, 2001). An elitist genetic algorithm always favours individuals with better fitness value and a controlled NSGA-II helps increasing the diversity of the population and forms a better PoF. The algorithm takes an initial population from a surrogate and proceeds through generations via mutations and crossovers. The initial population is called a parent population and initially the points are selected arbitrarily. The objective function values are estimated at each design through actual estimation of CFD or via surrogate model. Finally, the stopping criterion reaches to accept the converged solution. In the present computation, fifty generations were set as stopping criterion and PoF was generated. Some of the Pareto-optimal solutions were selected via clustering and reproduced through RANS analysis.

NSGA-II requires a large number of initial populations, which are expensive to evaluate by a high fidelity CFD model. An easy way to reduce such expenses is to construct a cheaper model or surrogate and generate the population from the surrogate. A higher error in a surrogate may lead to a poor relationship between the objectives. The CV error estimation gives an idea of the goodness of surrogate fitting and helps finding weights (Eq. (4)) for the basic surrogates. The feasible solutions are plotted in PoF, and the points are clustered by k-means clustering algorithm.

4. Result and discussion

4.1. Validation of numerical results

The CFD simulations are considered as the 'high-fidelity' simulations and need to be validated with the existing standard experimental or numerical models. The present results have been compared with other CFD (Torresi et al., 2008) and experimental (Curran and Gato, 1997) results. The static pressure coefficient (ΔP^*), the torque coefficient (T^*), and the efficiency (η) are plotted for a wide range of flow coefficient. Fig. 8 shows that the present results match well with the existing results.

After validation, the ranges of the variables were fixed through some initial computations or through the designer's experience. For example, $\lambda_{tip} = -20°$ and $\lambda_{mid} = 20°$ yielded a completely impractical design. In some cases, the convergence in the optimization algorithm was not achieved. Hence, the angles (λ_{tip} and λ_{mid}) were changed iteratively and finally a feasible design space was created. Nine sample points (or design points) were selected within the design space (Table 4).

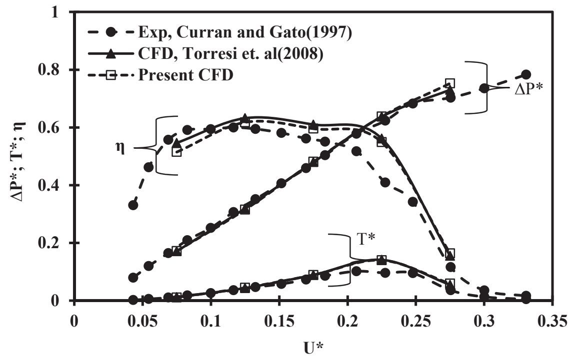

Fig. 8. Validation with experimental and numerical results.

The designs distributed in the design space were simulated using the CFD solver to estimate the objective function values.

A surrogate's fidelity depends upon the nature of the data points used in its construction. Several surrogates were constructed and the errors (E_i in Eq. (4)) were evaluated (Table 5). The table shows that the objective functions have the same surrogate (RBF) which produced least errors for this problem. Prior to this calculation, it was unclear which surrogate produced the least error. Finally, the weighted average surrogates were constructed using the Eq. (3). It was observed that the RBF fetched the highest weight (w); whereas, the KRG got the least for both the surrogates. However, it was not always true that the RBF or KRG had the highest or lowest errors, respectively (Badhurshah and Samad, 2015; Bellary et al., 2014). The surrogate WAS was constructed twice (one for T^* and another for η) and the surrogates were used to generate initial populations for the NSGA-II.

Table 6 shows that the cluster points were obtained from the NSGA-II. Five cluster points were selected and the same points were evaluated again using the CFD solver. These points were sequentially named as A, B, C, D and E. Where, point A shows the highest peak-torque coefficient ($=T^*$) and lowest efficiency value ($=\eta$) (Fig. 9) while point E shows the lowest T^* and the highest ηin the present design. The results differ owing to the errors induced in both the surrogates and NSGA-II predictions.

Fig. 9 shows the relationship between the objectives. The high efficiency design has a lower peak-torque. The reference point is located nearby point D and the other points lie at the left or right side of the PoF.

Fig. 10 shows the CFD computed results for a wider U^* for all the cluster points. As the turbine diameter or the hub diameter does not change, the resistance to fluid flow is almost similar for all the designs and increases with U^*. The pressure drop across the turbine varies linearly with flow rate because of the increase in the energy exchange. Fig. 10a and b shows that the torque coefficient and efficiency are different design point for all the cases. The reference case has a lower peak-

Table 5
Weights for the surrogates to construct WAS.

Objective functions	CV error		
	KRG	RSA	RBF
T^*	0.058	0.042	0.034
η	0.066	0.053	0.035

Table 6
WAS—WAS results at different clustered points.

Points	$\lambda^o{}_{mid}$	$\lambda^o{}_{tip}$	NSGA-II predicted results		CFD predicted results	
			$\eta_{,NSGA}$	$T^*_{,NSGA}$	$\eta_{,CFD}$	$T^*_{,CFD}$
A	4.6	−6.70	0.498	0.201	0.465	0.201
B	−4.7	−6.90	0.530	0.184	0.473	0.186
C	−4.7	−3.20	0.539	0.162	0.507	0.139
D	−2.2	−0.27	0.542	0.137	0.539	0.142
E	3.9	8.70	0.567	0.099	0.572	0.084
Ref	0.0	0.00	—	—	0.538	0.138

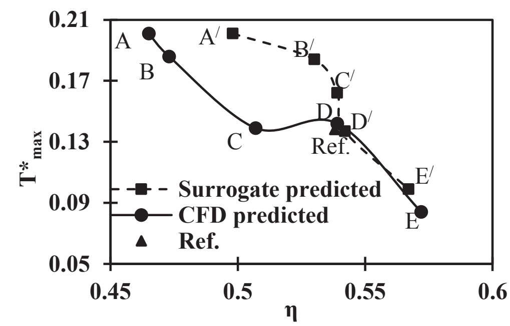

Fig. 9. Pareto optimal designs showing five cluster points only.

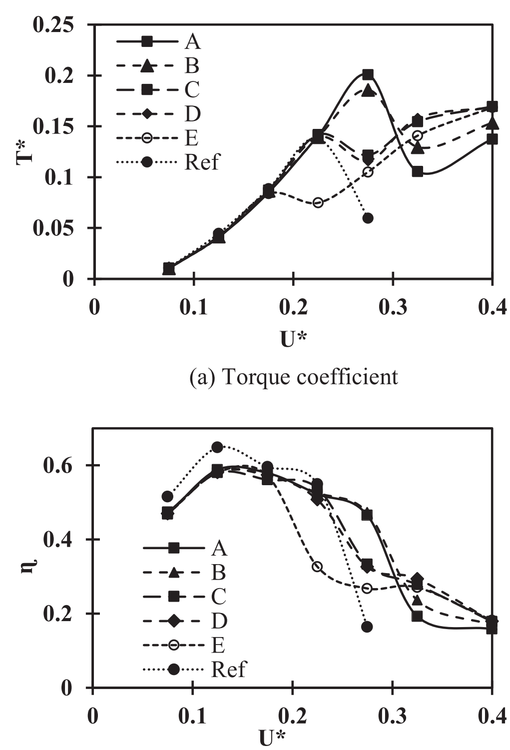

(a) Torque coefficient

(b) Efficiency

Fig. 10. Effect of blade sweep.

Please cite this article in press as: Halder, P., et al., Numerical optimization of Wells turbine for wave energy extraction, International Journal of Naval Architecture and Ocean Engineering (2016), http://dx.doi.org/10.1016/j.ijnaoe.2016.06.008

torque and a lower operating-range. Nevertheless, the efficiency is slightly higher in the reference case.

Fig. 11 shows the improvement in power output of the optimized blade. The Maximum enhancement in power (=28.8%) is achieved in design A. The unswept blade has η_{max} = 0.648 at U^* = 0.125 and stalled at U^* = 0.225 (Fig. 12). The design A performs better as compared to design E in terms of peak-torque enhancement, which conforms the existing results (Brito-Melo et al., 2002; Webster and Gato, 1999a,b; Suzuki and Arakawa, 2008).

For further analysis, only two designs (A and E) from the PoF are selected and detailed CFD analysis is presented below.

4.2. Internal flow analysis

Fig. 13 illustrates the comparison of static pressure coefficients at the mid-section of the flow passage for the Ref, A, and E designs. The pressure is almost constant at lower U^* (=0.125) on both the surfaces (PS and SS). As the FC increases, the pressure coefficient also increases. At higher U^* (=0.275), a higher pressure zone appears on the PS of the design A, while a lower pressure zone appears on the suction surface (SS) for Ref and E. Ref shows a drastic drop in efficiency (Fig. 10b) because of the large flow separation. Again, E has a lower efficiency than A at $U^* = 0.275$ (Figs. 10b and 13). A lower pressure region on SS of E covers more area than that of A. This low pressure promotes flow separation and gives lower efficiency.

Fig. 14 shows the streamlines patterns at mid-span of the flow passage near TE. At lower U^* (=0.125). The flow is attached to the SS and the efficiency remains almost same for all the cases. The flow separation increases with the increase in U^*. At higher U^* (=0.275), the separation region is near the TE on SS of A and E because of the low pressure on SS (Fig. 13). Ref shows a wider flow separation zone which gives a low efficiency (Figs. 10b and 14). In E for $U^* = 0.275$, two vortex appeared near the TE, flow separation zone became larger, and a lower efficiency was obtained as compared to case A.

The streamline patterns on SS shows a lower flow separation and same efficiency at a lower U^* (=0.125) in all the cases (Fig. 15). For a turbine operating at a constant speed with a low flow rate, the aerofoil gets the highest lift as the flow is attached. The low velocity fluid particles possess lower

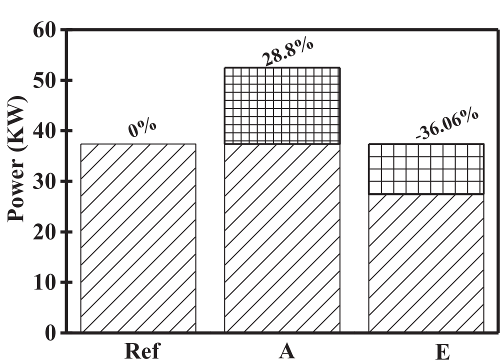

Fig. 11. Power output of designs: Ref, A and E.

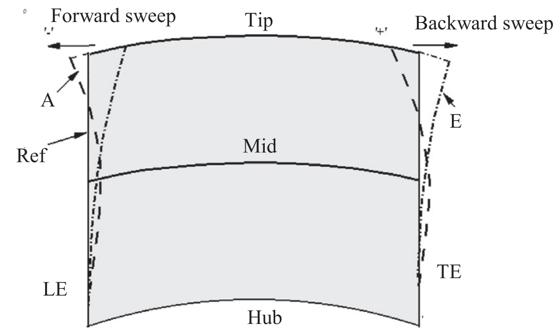

(a)Reference blade is the shaded one, Blade A and the blade E

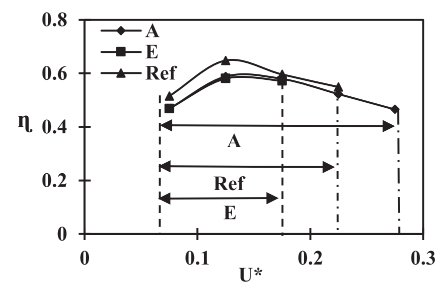

(b)Operating range

Fig. 12. Optimized blades and their operating ranges.

kinetic energy and hence, the total efficiency or the power transfer to the aerofoil is low. Small flow separation zone is visible near the hub of TE and it leads to the inception of smaller vortices. A further increase in flow velocity increases the separation zone. At this point, we get the highest torque. An increase in flow rate increases the angle of attack for a given rotational speed.

Fig. 16 shows the circumferential velocity contours for blade to blade passage at the blade mid-span. SS has a thinner boundary layer attached to the blade surface at a lower flow coefficient ($U^* = 0.125$). As the flow coefficient increases, the boundary layer thickness increases due to increase in angle of attract, and a wake appears at TE and gets deflected towards the axial direction. A higher velocity region is noticed near the LE of A. Because of the blade sweep, the distribution of the flow is not perpendicular to the spans, hence the streamline curvature is different for both SS and PS.

Fig. 17 represents a line from hub to tip at downstream of the flow. The line is located at the mid-chord. The static pressure distribution at the line is shown in Fig. 18. At a lower flow coefficient ($U^* = 0.125$), a lower pressure is found near the blade tip for Ref. At a higher angle of attack, a lower pressure is observed near the hub of Ref as compared to the other designs. The pressure distribution gradually decreases with the span for A.

Fig. 19 shows the axial velocity distribution along the blade span. At the lower flow coefficient ($U^* = 0.125$), the velocity distribution is almost same for all the cases as the angle of attack is low (Fig. 16). At the higher flow coefficient ($U^* = 0.275$), the velocity is high for Ref while it is low for A and E near the hub.

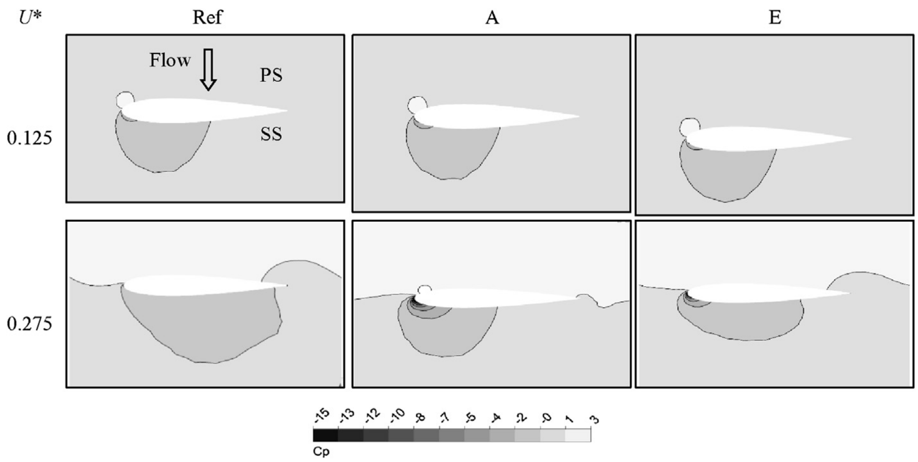

Fig. 13. Pressure contours at different flow coefficients.

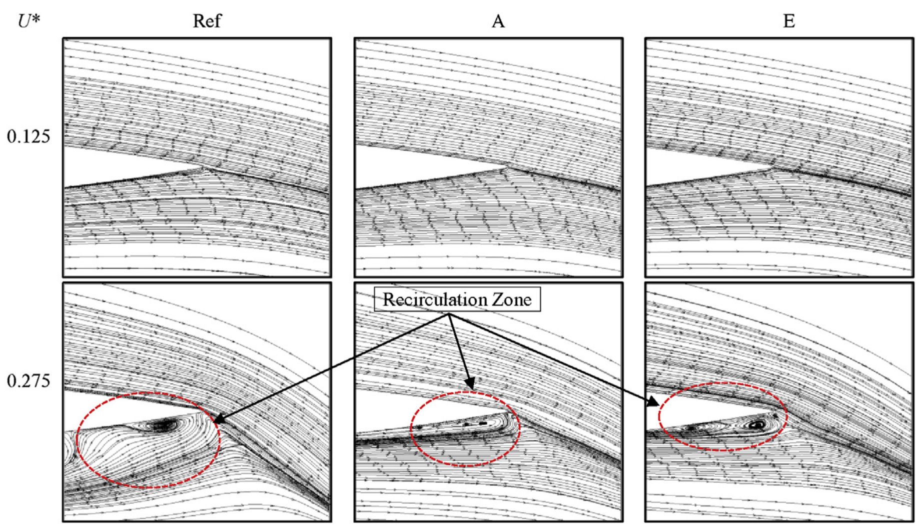

Fig. 14. Streamline lines that show the recirculation zone at the blade mid-span near TE.

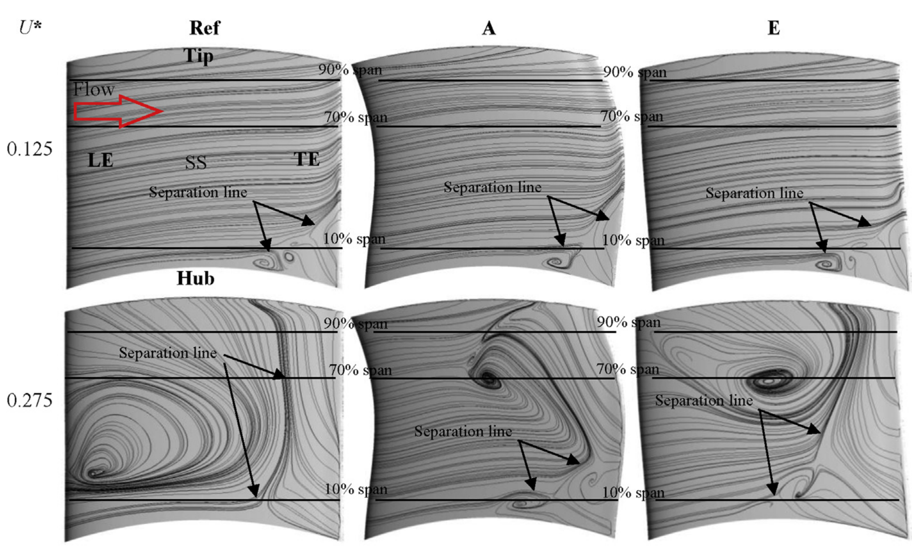

Fig. 15. Streamlines on the blade suction surface.

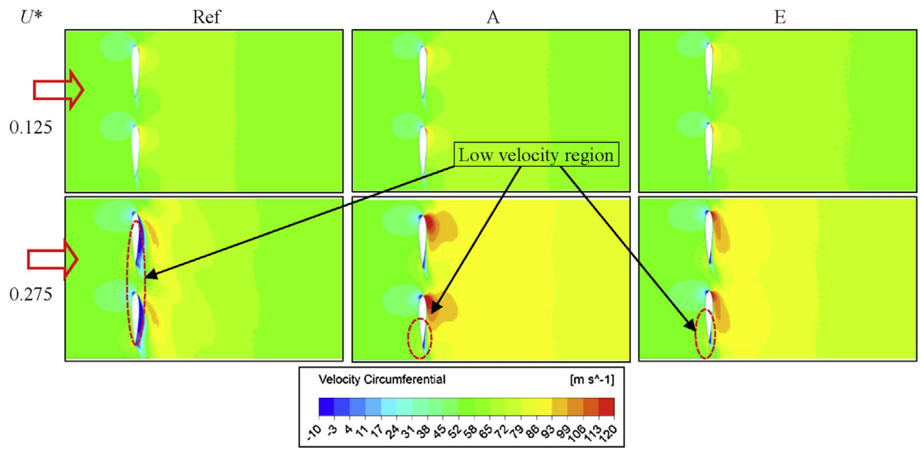

Fig. 16. Circumferential velocity contours for blade to blade at the mid-span.

5. Conclusions

Numerical analyses by solving the RANS equations with *k-w* SST model and multi-objective optimization of Wells turbine blade have been carried out in the present work. The computational results are validated with the existing experimental and numerical results and it is found that the results are well matched. Nine design points are selected in the design space by using full factorial. A weighted-average surrogate based genetic algorithm has been implemented and multiple optimal designs are produced in a Pareto optimal solutions. Some cluster points are verified with CFD analyses.

From the solution, only two extreme designs, design A and design E, are selected. It is found that a higher efficiency design may not yield a higher peak-torque design. The design A has a backward sweep at the mid-section and a forward sweep at the

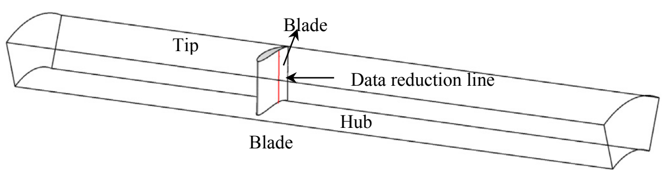

Fig. 17. Data reduction line at the downstream of the blade.

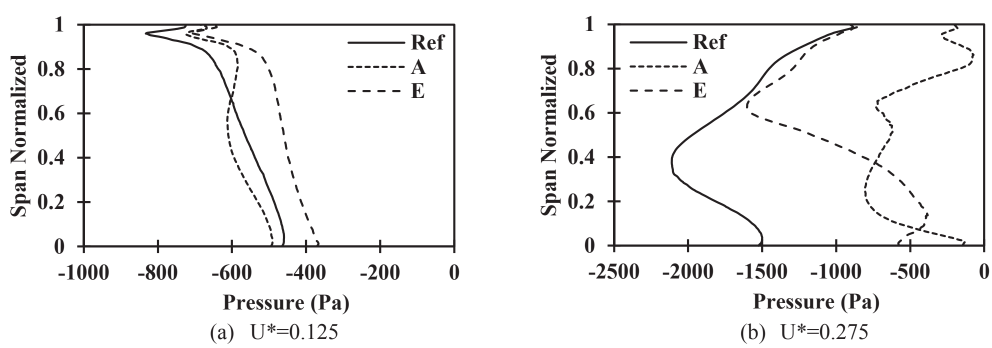

Fig. 18. Static pressure distribution mid-chord of the blade span.

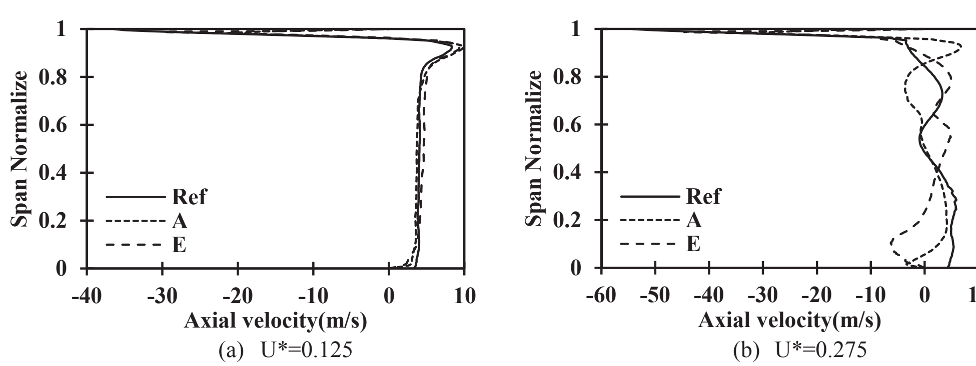

Fig. 19. Axial velocity distribution along the blade span wise.

Please cite this article in press as: Halder, P., et al., Numerical optimization of Wells turbine for wave energy extraction, International Journal of Naval Architecture and Ocean Engineering (2016), http://dx.doi.org/10.1016/j.ijnaoe.2016.06.008

tip-section of the blade and gives a higher power output. The peak torque-coefficient increases by 28.28% and the corresponding efficiency decreases by 13.5%. However, the operating-range increases by 18.18%. In design E, the peak-torque coefficient decreases by 36% and the corresponding efficiency increases by 6% as compared to the reference design. The operating range decreases by 22.22%. The blade A has a smaller separation region at the TE than the reference blade and blade E and has a higher torque than the unswept blade. The change in flow separation is responsible for efficiency change.

Acknowledgement

This work was supported by Brain Pool Program through the Korean Federation of Science and Technology Societies (KOFST) funded by the Ministry of Science, ICT and Future Planning.

References

Ansys CFX, 2010. Release 11.0: Ansys CFX-solver Theory Guide. ANSYS.
Badhurshah, R., Samad, A., 2015. Multiple surrogate based optimization of a bidirectional impulse turbine for wave energy conversion. Renew. Energy 74, 749−760. http://dx.doi.org/10.1016/j.renene.2014.09.001.
Bellary, S.A.I., Husain, A., Samad, A., 2014. Effectiveness of meta-models for multi-objective optimization of centrifugal impeller. J. Mech. Sci. Technol. 28, 4947−4957.
Benini, E., Biollo, R., 2007. Aerodynamics of swept and leaned transonic compressor-rotors. Appl. Energy 84, 1012−1027. http://dx.doi.org/10.1016/j.apenergy.2007.03.003.
Brito-Melo, A., Gato, L.M.C., Sarmento, A.J.N.A., 2002. Analysis of Wells turbine design parameters by numerical simulation of the OWC performance. Ocean. Eng. 29, 1463−1477. http://dx.doi.org/10.1016/S0029-8018(01)00099-3.
Collette, Y., Siarry, P., 2003. Multiobjective optimization: principles and case studies. Decision Engineering. Springer Science & Business Media. http://dx.doi.org/10.1007/978-3-662-08883-8.
Curran, R., Gato, L.M.C., 1997. The energy conversion performance of several types of Wells turbine designs. Proc. Inst. Mech. Eng. Part A J. Power Energy 211, 133−145. http://dx.doi.org/10.1243/0957650971537051.
Deb, K., 2001. Multi-objective Optimization Using Evolutionary Algorithms. John Wiley & Sons.
Gato, L.M.C., Webster, M., 2001. An experimental investigation into the effect of rotor blade sweep on the performance of the variable-pitch Wells turbine. Proc. Inst. Mech. Eng. Part A J. Power Energy 215, 611−622. http://dx.doi.org/10.1243/0957650011538848.
Goel, T., Haftka, R.T., Shyy, W., Queipo, N.V., 2007. Ensemble of surrogates. Struct. Multidiscip. Optim. 33, 199−216. http://dx.doi.org/10.1007/s00158-006-0051-9.
Gorissen, D., Couckuyt, I., Laermans, E., Dhaene, T., 2010. Multiobjective global surrogate modeling, dealing with the 5-percent problem. Eng. Comput. 26, 81−98. http://dx.doi.org/10.1007/s00366-009-0138-1.
Halder, P., Samad, A., Kim, J.H., Choi, Y.S., 2015. High performance ocean energy harvesting turbine design−a new casing treatment scheme. Energy 86, 219−231. http://dx.doi.org/10.1016/j.energy.2015.03.131.
Jeong, S., Murayama, M., Yamamoto, K., 2005. Efficient optimization design method using kriging model. J. Aircr. 42, 413−420. http://dx.doi.org/10.2514/1.C10485E.
Kim, T., Setoguchi, T., Kinoue, Y., Kaneko, K., 2001. Effects of blade geometry on performance of wells turbine for wave power conversion. J. Therm. Sci. 10, 293−300. http://dx.doi.org/10.1007/s11630-001-0035-4.
Kim, T.H., Setoguchi, T., Kaneko, K., Raghunathan, S., 2002. Numerical investigation on the effect of blade sweep on the performance of Wells turbine. Renew. Energy. http://dx.doi.org/10.1016/S0960-1481(00)00210-X.
Marjavaara, D.B., Lundström, S.T., Goel, T., Mack, Y., Shyy, W., 2007. Hydraulic turbine diffuser shape optimization by multiple surrogate model approximations of pareto fronts. J. Fluids Eng. 129, 1228. http://dx.doi.org/10.1115/1.2754324.
Martin, J.D., Simpson, T.W., 2005. Use of kriging models to approximate deterministic computer models. AIAA J. 43, 853−863. http://dx.doi.org/10.2514/1.8650.
Matrices, S., 2012. The Language of Technical Computing. MathWorks, Inc., pp. 4−9. http//www.mathworks.com
Mohamed, M.H., Janiga, G., Pap, E., Thévenin, D., 2011. Multi-objective optimization of the airfoil shape of Wells turbine used for wave energy conversion. Energy 36, 438−446. http://dx.doi.org/10.1016/j.energy.2010.10.021.
Mohamed, M.H., Shaaban, S., 2013. Optimization of blade pitch angle of an axial turbine used for wave energy conversion. Energy 56, 229−239. http://dx.doi.org/10.1016/j.energy.2013.04.035.
Mohamed, H.M., Shaaban, S., 2014. Numerical optimization of axial turbine with self-pitch- controlled blades used for wave energy conversion. Int. J. Energy Res. 38, 592−601. http://dx.doi.org/10.1002/er.
Myers, R.H., Montgomery, D.C., 1995. Response Surface Methodology: Process and Product Optimization Using Designed Experiments. Wiley. John Wiley & Sons, New York. http://dx.doi.org/10.1016/S0378-3758(97)81631-X.
Orr, M.J.L., 1996. Introduction to Radial Basis Function Networks.
Raghunathan, S., 1995. The Wells air turbine for wave energy conversion. Prog. Aerosp. Sci. 31, 335−386. http://dx.doi.org/10.1016/0376-0421(95)00001-F.
Raghunathan, S., Tan, C.P., 1985. Effect of blade profile on the performance of the Wells self-rectifying air turbine. Int. J. Heat. Fluid Flow. 6, 369−379. http://dx.doi.org/10.1016/0142-727X(85)90026-8.
Sacks, J., Welch, W.J., Mitchell, T.J., Wynn, H.P., 2012. Design and analysis of computer experiments. Stat. Sci. 4, 409−423. http://dx.doi.org/10.1214/ss/1177012413.
Samad, A., Kim, K.Y., 2008. Shape optimization of an axial compressor blade by multi-objective genetic algorithm. Proc. Inst. Mech. Eng. Part A J. Power Energy 222, 599−611. http://dx.doi.org/10.1243/09576509JPE596.
Samad, A., Kim, K.Y., Goel, T., Haftka, R.T., Shyy, W., 2008. Multiple surrogate modeling for axial compressor blade shape optimization. J. Propuls. Power 24, 301−310. http://dx.doi.org/10.2514/1.28999.
Simpson, T.W., Mauery, T.M., Korte, J., Mistree, F., 2001. Kriging models for global approximation in simulation-based multidisciplinary design optimization. AIAA J. 39, 2233−2241. http://dx.doi.org/10.2514/3.15017.
Suzuki, M., Arakawa, C., 2008. Influence of blade profiles on flow around Wells turbine. Int. J. Fluid Mach. Syst. 1, 148−154. http://dx.doi.org/10.5293/IJFMS, 1.1.148.
Taha, Z., Sugiyono, Sawada, T., 2010. A comparison of computational and experimental results of Wells turbine performance for wave energy conversion. Appl. Ocean. Res. 32, 83−90. http://dx.doi.org/10.1016/j.apor.2010.04.002.
Takao, M., Setoguchi, T., Kinoue, Y., Kaneko, K., 2007. Wells turbine with end plates for wave energy conversion. Ocean. Eng. 34, 1790−1795. http://dx.doi.org/10.1016/j.oceaneng.2006.10.009.
Takao, M., Thakker, A., Abdulhadi, R., Setoguchi, T., 2006. Effect of blade profile on the performance of a large-scale Wells turbine for wave-energy conversion. Int. J. Sustain. Energy 25, 53−61. http://dx.doi.org/10.1080/14786450600593295.
Thakker, A., Abdulhadi, R., 2007. Effect of blade profile on the performance of Wells turbine under unidirectional sinusoidal and real sea flow conditions. Int. J. Rotat. Mach. 2007 http://dx.doi.org/10.1155/2007/51598.
Torresi, M., Camporeale, S.M., Pascazio, G., Fortunato, B., 2004. Fluid Dynamic Analysis of a Low Solidity Wells Turbine. In: 59 Congresso ATI, Genova, Italy.
Torresi, M., Camporeale, S.M., Strippoli, P.D., Pascazio, G., 2008. Accurate numerical simulation of a high solidity Wells turbine. Renew. Energy 33, 735−747. http://dx.doi.org/10.1016/j.renene.2007.04.006.

Valipour, M., Banihabib, E., Behbahani, R., 2012. Monthly inflow forecasting using autoregressive artificial neural network. J. Appl. Sci. 12, 2139−2147.

Valipour, M., Banihabib, M.E., Behbahani, S.M.R., 2013. Comparison of the ARMA, ARIMA, and the autoregressive artificial neural network models in forecasting the monthly inflow of Dez dam reservoir. J. Hydrol. 476, 433−441. http://dx.doi.org/10.1016/j.jhydrol.2012.11.017.

Valipour, M., Montazar, A., 2012a. An evaluation of SWDC and WinSRFR models to optimize of infiltration parameters in furrow irrigation. Am. J. Sci. Res. 69, 128−142.

Valipour, M., Montazar, A.A., 2012b. Optimize of all effective infiltration parameters in furrow irrigation using visual basic and genetic algorithm programming. Aust. J. Basic Appl. Sci. 6, 132−137.

Valipour, M., Montazar, A.A., 2012c. Sensitive analysis of optimized infiltration parameters in SWDC model. Adv. Environ. Biol. 6, 2574−2581.

Wang, D., Bai, J.Q., Hua, J., Sun, Z.W., Qiao, L., 2014. Aerodynamic shape optimization design of the swept wing based on the kriging surrogate model. Appl. Mech. Mater. 444, 1277−1282.

Webster, M., Gato, L.M.C., 2001. The effect of rotor blade shape on the performance of the Wells turbine. Int. J. Offshore Polar Eng. 11, 227−230. http://dx.doi.org/10.1016/S0960-1481(00)00163-4.

Webster, M., Gato, L.M.C., 1999a. The effect of rotor blade sweep on the performance of the Wells turbine. Int. J. Offshore Polar Eng. 9, 233−240. http://dx.doi.org/10.1016/S0960-1481(00)00163-4.

Webster, M., Gato, L.M.C., 1999b. The effect of rotor blade shape on the performance of the Wells turbine. In: Proceedings of the Ninth (1999) International Offshore and Polar Engineering Conference. Brest, France, May 30-June 4, 1999, pp. 169−173. http://dx.doi.org/10.1016/S0960-1481(00)00163-4.

Please cite this article in press as: Halder, P., et al., Numerical optimization of Wells turbine for wave energy extraction, International Journal of Naval Architecture and Ocean Engineering (2016), http://dx.doi.org/10.1016/j.ijnaoe.2016.06.008